Cureus Journal of Engineering

Open Access Original Article

Static Deflection and Free Vibration Analysis of Functionally Graded Al-Al_2O_3 Clamped-Free Beams Fabricated by Powder Metallurgy

Pravin Malik [1] , Ravikiran Kadoli [1] , Sharnappa Joladarashi [1] , Permi Jagadish [1]

1. Department of Mechanical Engineering, National Institute of Technology Karnataka Surathkal, Mangalore, IND

Corresponding author: Pravin Malik, pravin_malik@yahoo.com

Received 03/18/2025
Review began 03/20/2025
Review ended 04/02/2025
Published 04/14/2025

DOI: https://doi.org/10.7759/s44388-025-03835-2

Abstract
This study examines the static deflection and free vibration behavior of functionally graded aluminium-alumina (Al-Al_2O_3) beams fabricated using the powder metallurgy process. Three different beam configurations with 5, 6, and 7 layers, incorporating ceramic volume fractions of 10%, 20%, and 50% in the outermost layer, are considered. Experiments are conducted on the Al-Al_2O_3 beams with clamped free boundary condition for their static deflections and natural frequencies. These experimental results are compared with the numerical estimates obtained using beam finite element. Porosity models have been considered to evaluate material properties like density and Young's modulus. Two distinct porosity models were used to assess numerical static deflections and natural frequencies. The results show a significant increase in the error between experimental and numerical static deflections, rising from 30% to 80%, while the free vibration frequencies increased from 10% to 75%. These changes occurred as the ceramic volume fraction increased from 10% to 50% for the Al-Al_2O_3 beams examined in the study. This highlights the need for refining the powder metallurgy process to minimize porosity and improve material consistency.

Categories: Advanced Manufacturing Technologies, Advanced Materials, Materials Engineering
Keywords: free vibration, static deflection, metal-ceramic functionally graded beam, porosity, powder metallurgy process, power law index, rule of mixture

Introduction
Functionally graded structures are those in which the volume fractions of two or more materials are varied continuously as a function of position along certain dimension(s) of the structure. A typical functionally graded material (FGM) for high temperature applications is synthesized from a mixture of ceramic and metal. The material properties in these materials do not vary suddenly from one surface to another and thus there are good chances of reducing the mechanical and thermal stress concentrations. Accordingly, FGMs are suitable for engineering applications and are good replacement for the laminated composite structures. However, the challenges in the manufacturing techniques are multitude in nature, especially production of defect-free products. Powder metallurgy and thermal spray have been the most widely used processes for fabricating FGMs. These processes are recognized for their versatility, providing excellent control over microstructure. However, there is a lack of comprehensive studies on the fabrication of FGMs using these techniques, particularly with aluminium and alumina as the FGM constituent materials. Gupta and Talha [1] have reviewed various fabrication methods for FGMs and outlined future research directions that could help in the design and analysis of these materials. A review of a variety of manufacturing processes attempted for fabricating FGM is made available by Kieback et al. [2], Sobczak and Drenchev [3] as well as Naebe and Shirvanimoghaddam [4]. The review also describes the microstructural features of the graded structures and the necessity of adopting modeling of the manufacturing process so that process parameters can be established to reduce cost and defects in the graded products. A novel technique for the fabrication and fracture testing of large-scale polymeric-based FGMs has been presented by Lambros et al. [5]. They showed that, for specimens over 150 mm thickness, the FGMs produced by this process exhibit a varying Young's modulus, from approximately 160 to 250 MPa. Saleh et al. [6] provided an overview of design and manufacturing techniques for smooth graded FGMs, outlining the key challenges and advantages of these methods based on over 30 years of available literature. Boggarapu et al. [7] studied the mechanical and tribological properties of a five-layered Al/Cu FGM produced by powder metallurgy. Gupta et al. [8] have investigated how sintering temperature and time influence the properties of Fe-Al_2O_3 composites produced through the powder metallurgy process. Bhattacharyya et al. [9] studied microstructure, micro-hardness, porosity content, and flexural strength of functionally graded (FG) beams fabricated from Al-SiC combination and Ni-Al_2O_3 combination, with ceramic volume varying from 10% to 40%.

During the study of FGMs with regards to static deflection, and vibration, apart from preparation of the specimens, it is necessary to have knowledge of arriving at the physical properties of the graded structure.

Especially graded materials prepared by powder compaction process, the physical properties strongly depend on the porosity of the specimens. Matuła et al. [10] developed an innovative powder metallurgy method for producing functional, two-zoned graded materials with variable porosity. Phani and Niyogi [11] developed semi-empirical relation to calculate the material property of alumina depending on the magnitude of porosity and the same was compared with many other existing porosity-elastic modulus expressions available in literature. Asmani et al. [12] describes the use of the wave velocity data in formulating the effect of porosity, pore size, and distribution on the elastic modulus for alumina pellets. Kováčik [13] proposes the percolation theory to evaluate Young's modulus dependency on porosity. Chawla and Deng [14] studied the porosity effect on the Young's modulus, microstructure, tensile strength, strain-to-failure, and fatigue strength for Fe-0.85Mo-Ni steels prepared by powder metallurgy process. Savchenko et al. [15] carried out compression experiments on alumina cylindrical ingots with different porosity levels and studied the influence of porosity on shear strength, shear modulus, and modulus of elasticity. Wattanasakulpong and Ungbhakorn [16] incorporated the effects of porosity into the rule of mixtures (ROMs) and presented results on how varying porosity levels influence the frequency response of FG beams. Studies on the free vibration of FG beams prepared by hot isostatic pressing, sequential infiltration technique, and plasma spray process has been presented by Kapuria et al. [17], Wattanasakupong et al. [18], and Malik and Kadoli [19], respectively.

To the best of the author's knowledge, no studies have been reported on the experimental static deflection and natural frequencies of Al-Al_2O_3 FG beams, processed through powder metallurgy, under a clamped-free boundary condition. Additionally, a FORTRAN computer program has been developed using beam finite elements, along with the simple ROMs, power law index, and porosity models, to numerically evaluate static deflection and natural frequencies. A comparison of experimental and numerical results reveals discrepancies, with the error appearing to increase significantly when the ceramic volume fraction is high. This suggests that while porosity models and gradation laws are adequate for theoretical estimates, more stringent control of the manufacturing process is necessary.

Materials And Methods

Material gradation through the thickness of functionally graded beam

Consider an FG beam with rectangular cross section. Let l, b, and h be the length, width, and thickness of the beam. The x coordinate is considered at the mid-plane along the length of the beam and y coordinate is taken along the width of the beam. Figure *1* represents FG beam with stepwise material gradation. The material property of each layer is considered as per the ROM along the z direction. Each layer having a mixture of ceramic and metal with volume fractions V_c and V_m, and simple ROM holds true.

$$V_c + V_m = 1 \qquad (1)$$

The effective material property, P_{eff} for each layer of the stepwise graded FG beam is given by the relation

$$P_{eff}(z) = P_m V_m(z) + P_c V_c(z) \qquad (2)$$

where, P and V represents a physical property and volume fraction which varies along the thickness direction (z coordinate). Subscript c and m indicate ceramic and metal, respectively.

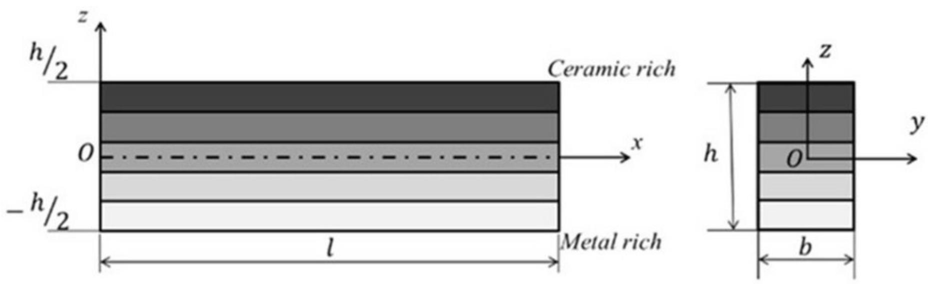

FIGURE 1: FG beam with stepwise gradation along its thickness

FG, functionally graded

Figure *2* represents FG beam with continuous gradation through thickness. The variation of the material property from metal rich to ceramic rich is continuous and the variation is along z axis. The variation of volume fraction of ceramic along the thickness is based on the power law index . The power law index takes on values greater than or equal to zero. The effective material property variation along the thickness direction based on power law variation for volume fraction of ceramic is given by:

$$P_{eff}(z) = (P_c - P_m)\left(\frac{z}{h} + \frac{1}{2}\right)^n + P_m \quad (3)$$

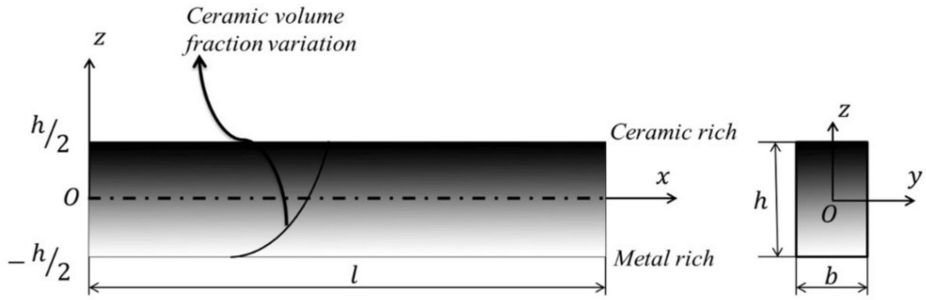

FIGURE 2: FG beam with continuous gradation through thickness

FG, functionally graded

Beam finite element formulation

The finite element equation of motion is derived following the discussion in Demir and Oz [20]. The elastic strain energy of a finite element is

$$U = \frac{1}{2}\int_0^L \left[A_{11}\left(\frac{\partial u_0}{\partial x}\right)^2 - 2B_{11}\left(\frac{\partial u_0}{\partial x}\right)\left(\frac{\partial^2 w_0}{\partial x^2}\right)^2 + D_{11}\left(\frac{\partial^2 w_0}{\partial x^2}\right)^2\right] dx \quad (4)$$

where A_{11} , B_{11} , and D_{11} are extensional rigidity, coupling rigidity, and bending rigidity defined as

$$A_{11}, B_{11}, D_{11} = \int_{Z_{k-1}}^{Z_k} Q_{11}\left(1, z, z^2\right) dz \quad (5)$$

z_k and z_{k-1} stand for the k^{th} and $(k-1)^{th}$ layer of the FG beam. The reduced stiffness coefficient Q_{11} in Equation (5) is calculated for each layer

$$Q_{11} = \frac{E_{eff}}{1 - \nu_{eff}^2} \quad (6)$$

E_{eff} and ν_{eff} namely, the effective Young's modulus and Poisson's ratio is computed according to Equation (2) or Equation (3).

Including the rotary inertia and the axial inertia effects, the kinetic energy of beam, K , at any instant can be expressed as

$$K = \frac{1}{2}\int_0^L \left[I_A\left(\frac{\partial u_0}{\partial t}\right)^2 - 2I_B\left(\frac{\partial u_0}{\partial t}\right)\left(\frac{\partial^2 w_0}{\partial x \partial t}\right) + I_D\left(\frac{\partial^2 w_0}{\partial x \partial t}\right)^2 + I_A\left(\frac{\partial w_0}{\partial t}\right)^2\right] dx$$

(7)

where I_A , I_B and I_D in Equation (7) are the inertial coefficient defined as

$$(I_A, I_B, I_D) = \int_{Z_{k-1}}^{Z_k} \rho(z)\left(1, z, z^2\right) b\,dz \quad (8)$$

$\rho(z)$ is the effective density of the layered or continuously graded beam.

The axial and transverse displacement u and w , respectively, are expressed in terms of nodal displacements by the Lagrange shape function and Hermite shape function. The shape functions are substituted into the elastic strain energy (Equation (4)) and kinetic energy (Equation (7)), and various stiffness and mass matrices are evaluated (Demir and Oz [20]). The finite element equation of motion is obtained as follows:

$$[K]\{q\} + [M]\{\ddot{q}\} = \{F\} \qquad (9)$$

$[K]$ and $[M]$ are the global stiffness and mass matrices of order 6 × 6. $\{F\}$ is the load vector.

Fabrication of functionally graded beams using powder metallurgy process

Al-Al_2O_3 FG beam samples having five layers were prepared by the powder metallurgy process. The thickness of each layer in the beam was approximately between 0.45 and 0.5 mm depending on the weight of the powder used for each layer. The ceramic content in the layers of the beam samples were from 0% to 10% with the bottom layer being of pure metal and the top layer having 10% ceramic content. The five layered FG beam sample had Al_2O_3 composition as 0/1.25/2.5/5/10% from bottom to top layer. The metal and ceramic constituents were mixed thoroughly in a planetary ball mill and laid layer by layer in a die. The powder laid in the die was compacted using a universal testing machine. After compaction, the samples were subjected to sintering. Liu [21] has investigated the impact of varying the sintering temperature from 600°C to 650°C on the relative density of aluminium during the sintering of aluminium powder. Based on Liu's findings, the sintering temperature in this work was increased to 650°C, which produced better samples that did not break when gently flexed manually. Further parametric studies were carried out by sintering FGM beam samples at furnace temperatures of 660°C, 670°C, and 680°C to arrive at the best possible sintering temperature for FGM samples. When the sintering temperature was raised to 670°C and 680°C, the aluminium layer melted and formed a lump, limiting the sintering process to 660°C. Rather than sintering the sample directly at 660°C, a step-wise increase in temperature was employed following the work of Pieczonka and Kazior [22]. The temperature was raised by 10°C per minute through manual adjustment of the control knob until it reached 660°C. The sintering temperature was varied linearly until the final sintering temperature of 660°C was attained. The length of the sample used in present study was 150 mm and had a cross section of 20 × 2.54 mm. The parameters used for preparing the Al-Al_2O_3 FGM beam samples using powder metallurgy process are listed in Table *1*.

Process parameter	Value
Die wall lubricant	Zinc stearate
Binding agent	Ethanol
Load applied	60 tons
Loading duration	5 min
Green compacting load	10 tons for 1 min
Sintering temperature	660°C
Stepwise increase of temperature	10°C per min
Sintering duration	5 hours
Cooling	Furnace cooling

TABLE 1: Parameters used for preparing the Al-Al2O3 FGM beam samples

FGM, functionally graded material

Figure *3* shows the beam sample consisting of five layers, with the extreme layer having a ceramic volume fraction of 10%. Al_2O_3 content in the beam layers is characterized by an appearance similar to granules. Traversing from bottom to top along the picture (Figure *3*), it can be observed that the concentration of Al_2O_3 is visibly increasing. The morphology almost remains the same for all the FG beams that have this composition. Similarly, FG beams of 6 and 7 layers were produced, wherein the ceramic volume fraction was 20% and 50% on the ceramic-rich outer most layer. The thickness of each layer was again maintained between 0.4 mm to 0.5 mm. The details of the properties of the material considered for calculations are in Table *2*. The thickness depends on the weight of the powder. The average weight of the powder for pure aluminium layer is 3.4 g and for different FG layers it varies from 3.442 g to 4.8 g. A high-precision weighing balance (CONTECH electronic balance CAI-234) was used to measure the mass of the powder. Considering all these parameters, it is found that the beam thickness after fabrication is between 2.1 mm to 3.5 mm.

Material	Young's modulus, E (GPa)	Density, ρ (kg/m^3)	Poisson's ratio, v
Aluminium	69.0	2698	0.26
Alumina (Al_2O_3)	349.55	3750	0.33

TABLE 2: Material properties of aluminium and Al2O3

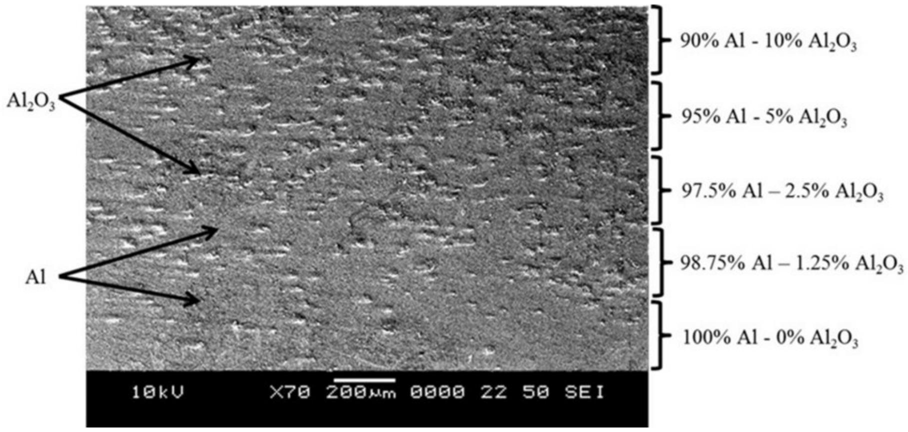

FIGURE 3: Microstructure SEM picture of FG-23

SEM, Scanning Electron Microscopy

Evaluation of porosity for FGM beam

FG beams prepared by powder metallurgy process containing porosity p can be evaluated from the equation presented by Phani and Niyogi [23]

$$p = \frac{\rho_T - \rho_A}{\rho_T} \qquad (10)$$

where ρ_T is the averaged theoretical density of each layer of the FG beam calculated using Equation (2) and ρ_A is the actual density calculated as $\rho_A = \frac{mass}{volume}$, where volume is evaluated using geometric quantities like length, width, and thickness of the FG beams.

In the hypothesis of pores presenting spheroid symmetry, the dependency of Young's modulus on porosity has been formulated by Asmani et al. [12] as

$$E(p) = E_T(1 - p^{2/3})^S \qquad (11)$$

E_T will be the theoretical Young's modulus of the material when porosity is zero. For FG beam E_T is E_{eff} and evaluated using Equation (2) applied for each layer. E_m and E_c are same as provided in Table *2*. The value of S is described by Asmani et al. [12] for a spherical shape pore.

Wattanasakulpong and Ungbhakorn [16] have accounted the porosity in the analytical relation for effective property following the ROMs as follows:

$$P = P_m\left(V_m - \frac{p}{2}\right) + P_c\left(V_c - \frac{p}{2}\right) \qquad (12)$$

p is the porosity volume fraction defined by Equation (10).

Experimental setup for static deflection analysis of FG beams

The schematic diagram that illustrates the measurement of static deflection of the clamped-free beam is shown in Figure *4*. The deflection of the beam was recorded using a laser optical displacement sensor, Micro-Epsilon - optoNCDT-1402-10, which has a resolution of 1 micron and sampling rate of 10 ms. The analog output from the sensor is communicated to the computer through an RS422 analog to digital USB converter. The readings are acquired in the computer using the ILD1402 software. A point load perpendicular to the beam length is applied at the free end of the beam. The deflection readings are taken at the free end of the beam. The difference in the readings before and after the application of the load is taken as the beam displacement. Standard weights of 50g, 70 g, 100 g, 130 g, and 150 g were used to apply the load at the free end.

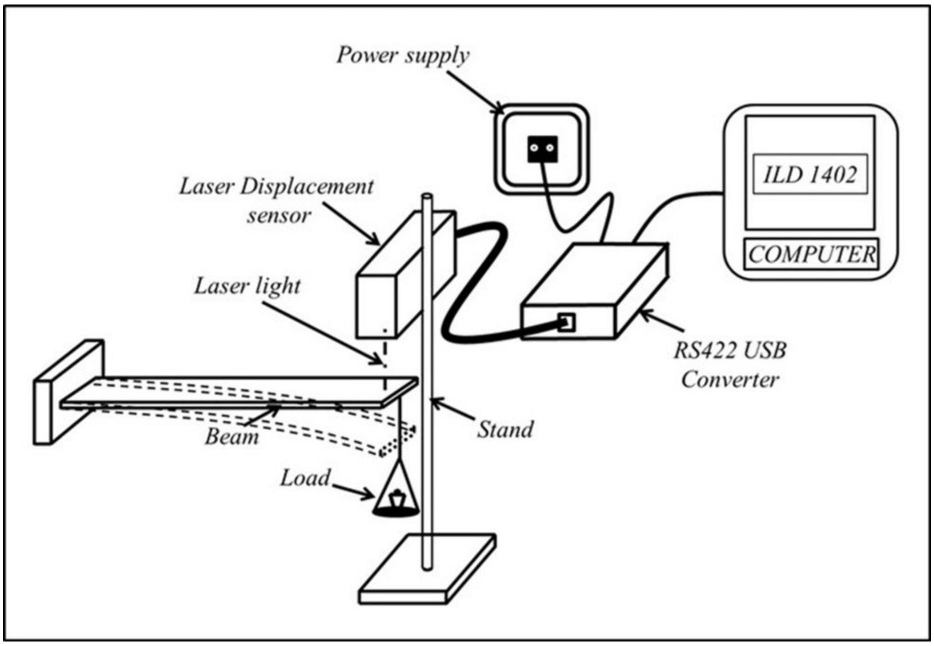

FIGURE 4: Schematic representation of experimental setup to measure the deflection of clamp-free beams

Experimental setup for free vibration natural frequency analysis of FG beams

The free vibration natural frequency of FG beams is determined using the impact hammer testing method. An impulse was given to the free end of the clamped-free beam as shown in Figure *5*. The response was recorded using a laser displacement sensor. The displacement signals from the laser sensor are recorded in the computer using the ILD1402 software. The FFT toolbox available in OriginPro 8 is used to obtain the frequency domain graph from the time domain plot for all samples. Alternatively, at different time intervals on the amplitude time curve, time period for one oscillation is measured. The reciprocal of the time period of one cycle is the frequency in Hertz.

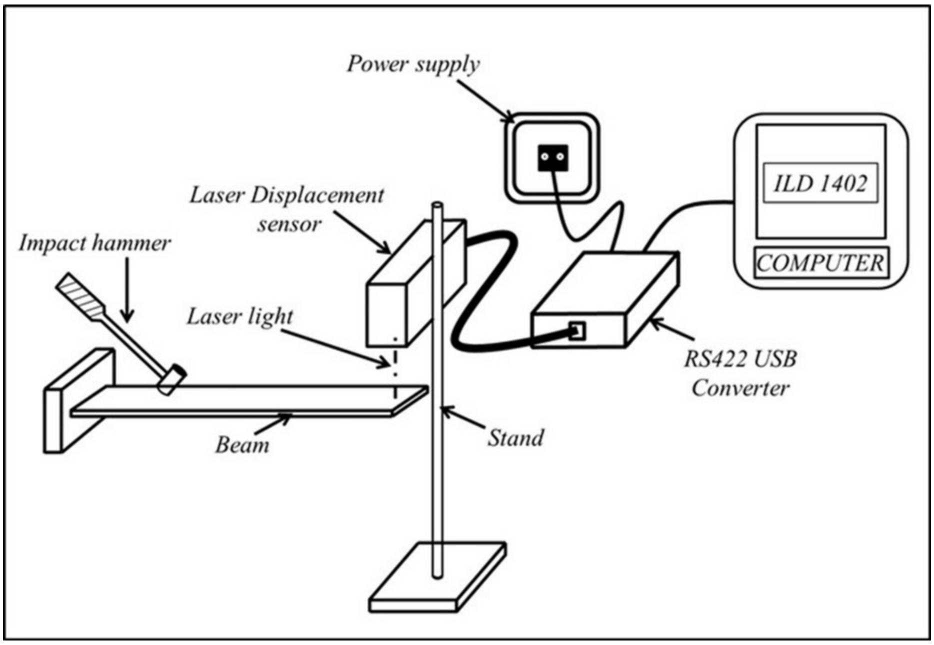

FIGURE 5: Schematic representation of experimental setup to measure the free vibration natural frequency of beams

Results

Analysis of porosity in FGM beam samples

The porosity calculated using Equation (10) are presented in Table *3* for the FG beams with maximum ceramic volume fraction of 10%, 20%, and 50% in the extreme layer. Referring to Table *3*, it can be observed that the porosity levels in the FG beams have increased as the ceramic volume fraction in the beam is increased. Few probable causes for porosity could be (i) entrapment of air during compaction of powder mixture, (ii) non-homogenous bonding of powder mixture, and (iii) unable to achieve sintering temperature close to that suitable for Al_2O_3 powder in the mixture. For most of the FG samples prepared, the layer containing more amount of Al_2O_3 powder, the surface corresponding to this layer had a powdery appearance or was coarse and dull. This observation is clearly supported, by physical inspection which shows that when the layer containing Al_2O_3 was felt by the fingers and when traversed over the surface, the powder would erode.

Sl. No.	FG beam sample	Actual density (kg/m^3)	Theoretical density (kg/m^3)	Porosity (%)
FG beams with maximum ceramic volume fraction of 10%				
1	FG-23	2412.53	2737.45	11.8
2	FG-24	2241.53	2737.45	18.1
3	FG-25	2323.77	2737.45	15.1
4	FG-38	2414.06	2737.45	11.8
FG beams with maximum ceramic volume fraction of 20%				
1	FG-28	2372.21	2765.94	14.2
2	FG-30	2360.51	2765.94	14.6
3	FG-36	2426.82	2765.94	12.2
4	FG-41	2404.13	2765.94	13.0
FG beams with maximum ceramic volume fraction of 50%				
1	FG-31	2293.51	2831.38	18.9
2	FG-35	2292.95	2831.38	19.0

TABLE 3: Porosity values for FG beam with various ceramic volume fraction

FG, functionally graded

Static deflection studies

The numerical results are calculated using the beam finite element FORTRAN computer program. Validation and convergence study of the computer program have been attempted. The number of finite elements used to obtain static deflection and free vibration frequency is 60. For the numerical calculations, the effective material property (i.e., the effective Young's modulus and effective density) for each layer of the stepped FG beams are calculated using Equation (2) i.e., the ROM. The effective beam length is the length from the fixed end to the free end of the beam which is equal to 130 mm.

The semi-empirical relation for Young's modulus and material density as a function of porosity proposed by Asmani et al. [12] and the one proposed by Wattanasakulpong and Ungbhakorn [16] are used to obtain static deflection of beams numerically. The comparison of static deflection from the experimental readings and the numerical results for a point load of 150 g at the free end are presented in Table *4*. Based on two approaches for calculating the material properties, the variation of static deflection increases with increase in load linearly, as seen in Figure *6*.

It is observed that Wattanasakulpong and Ungbhakorn [16] model and Asmani et al. [12] model for evaluation of Young's modulus and material density when used in the finite element program produced results which are close to one another. The error between numerical and experimental results for deflection has almost remained the same for the range of load applied for all the beams. The percentage errors are given in Table *4*. It is observed that the percentage error between the experimental and numerical results has increased when compared with the beams having maximum ceramic volume fraction of 10%.

Sl. No.	FG beam sample	Experimental deflection (mm)	Numerical deflection considering porosity (mm)		Percentage error (%)	
			Asmani et al. [12]	Wattanakulpong and Ungbhakorn [16]	Asmani et al. [12]	Wattanakulpong and Ungbhakorn [16]
FG beams with maximum ceramic volume fraction of 10%						
1	FG-23	1.303	0.911	0.915	30.07	29.71
2	FG-24	1.491	0.889	0.994	40.40	33.35
3	FG-25	1.305	0.982	1.036	24.72	20.63
4	FG-38	1.461	0.972	0.977	33.48	33.14
FG beams with maximum ceramic volume fraction of 20%						
1	FG-28	1.416	0.539	0.539	61.91	61.91
2	FG-30	1.193	0.484	0.477	59.39	60.00
3	FG-36	1.465	0.494	0.481	66.22	67.15
4	FG-41	1.312	0.503	0.488	61.62	62.76
FG beams with maximum ceramic volume fraction of 50%						
1	FG-31	0.871	0.171	0.153	80.32	82.34
2	FG-35	0.890	0.237	0.213	73.34	76.06

TABLE 4: Comparison of experimental static deflection of FG beams with the numerical results considering the effects of porosity

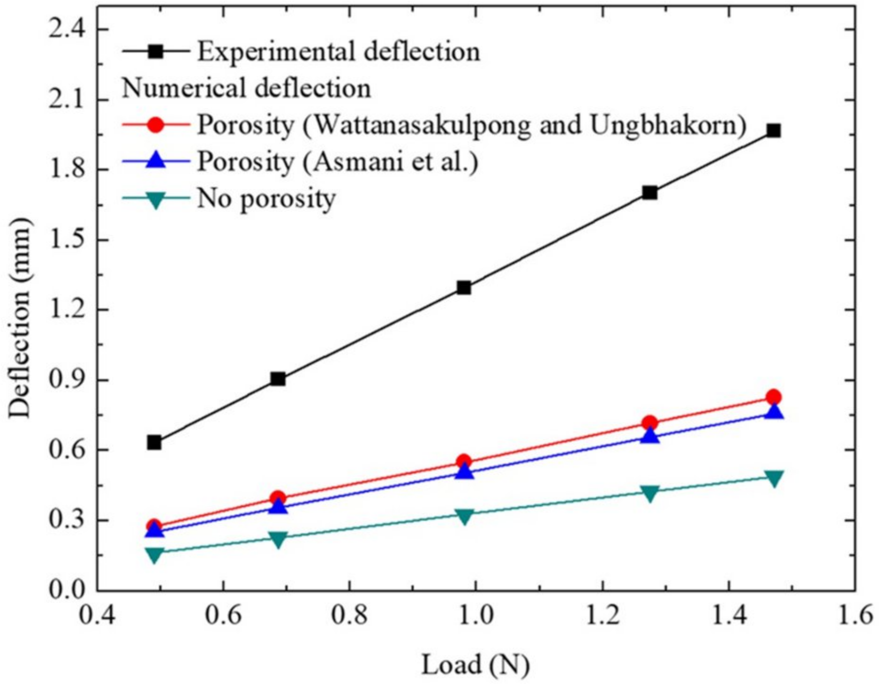

FIGURE 6: Comparison of the numerical deflection with experimental measurement for FG beam (FG-19) having maximum ceramic volume of 10%.

FG, functionally graded

Free vibration analysis

The natural frequency determined experimentally and calculated numerically from the finite element FORTRAN computer program, considering the effects of porosity, is presented in Table *5*. Consideration of porosity yields results that are closer to experimental results but yet far off. Using the Wattanasakulpong and Ungbhakorn [16] model to determine the physical properties yielded better results when compared to the results from the Asmani et al. [12] model.

Sl. No.	FG beam sample	Experimental frequency (Hz)	Numerical frequency considering effect of porosity (Hz)		Percentage error (%)	
			Asmani et al. [12]	Wattanasakulpong and Ungbhakorn [16]	Asmani et al. [12]	Wattanasakulpong and Ungbhakorn [16]
FG beams with maximum ceramic volume fraction of 10%						
1	FG-23	88.74	103.15	97.717	16.23	10.11
2	FG-24	87.65	102.56	91.94	17.01	4.89
3	FG-25	94.27	101.34	92.29	7.49	2.10
4	FG-38	85.97	100.68	95.43	17.11	11.00
FG beams with maximum ceramic volume fraction of 20%						
1	FG-28	79.35	124.99	118.49	57.52	49.32
2	FG-30	89.89	129.67	122.42	44.25	36.18
3	FG-36	83.13	128.08	123.64	54.06	48.72
4	FG-41	83.05	127.56	122.24	53.58	47.17
FG beams with maximum ceramic volume fraction of 50%						
1	FG-31	95.63	167.83	162.53	75.50	69.96
2	FG-35	93.16	171.29	165.63	83.85	77.78

TABLE 5: Free vibration natural frequency of Al-Al2O3 FG beams by considering the effects of porosity

FG, functionally graded

Discussion

Among the three types of Al-Al_2O_3 FG beams, it is important to note that the FG beam with a 50% ceramic volume fraction on the ceramic-rich side should exhibit greater stiffness compared to FG beams with 20% and 10% ceramic volume fractions. Both experimental and theoretical deflection results support this observation. However, several potential errors could affect the outcomes, such as improper bonding of particles between layers. One possible cause of this is an insufficient sintering temperature to achieve optimal bonding between the layers, as the melting temperature of alumina is significantly higher than that of aluminum. In the current study, a sintering temperature of 660°C was used, which is near the melting point of aluminum. When the sintering temperature was raised to 680°C, the aluminum layer melted and formed a lump, limiting the sintering process to 660°C.

This limitation on the sintering temperature prevents the proper fusion of alumina particles, which require temperatures between 1500°C and 1800°C for sintering. As a result, the presence of porosity and voids becomes evident. Porosity has a significant impact on the mechanical properties of the FG beams, such as Young's modulus and Poisson's ratio, which are key parameters in the theoretical models. Additionally, the bulk properties used in the models, derived from literature, may differ from those of the actual material used in the sample preparation. Accounting for porosity in the models yields results closer to the experimental data, but discrepancies still exist.

When applying the model by Wattanasakulpong and Ungbhakorn [16], better alignment with experimental results was observed compared to the model by Asmani et al. [12]. However, the error was still large, particularly for the FG beams with 20% and 50% ceramic volume fractions. As the ceramic volume fraction increases, the error becomes more pronounced. This can be attributed to improper densification due to the lower sintering temperatures, which do not adequately address the sintering needs of alumina. Consequently, as the alumina content in the beam increases, the error in the results also increases.

To optimize the performance of FG beams, particularly for structural applications, it is essential to minimize porosity levels by improving manufacturing techniques, such as more precise control over the sintering process. Further, microstructure studies need to be carried out in order to design a new porosity model for the Al-Al_2O_3 FGM beams. This porosity model needs to be incorporated in the theoretical model to arrive at the results close to the experimental results. Incorporating the effects of porosity into predictive models would improve the accuracy of material property estimations, such as Young's modulus and density, ultimately leading to better-designed FG structures.

Conclusions

The experimental results showed significant discrepancies between the measured static deflection and natural frequency when compared to the beam finite element analysis, despite accounting for porosity in the prepared samples. The static deflection and free vibration frequencies were within error limits of 30% and 10%, respectively, when the ceramic volume fraction was low (i.e., 10%). However, as the ceramic volume fraction increased, such as in the 20% and 50% cases, the error in static deflection and free vibration frequencies became significantly larger, more than 50%. This suggests a need for refinement in the powder metallurgy process, particularly in controlling the sintering temperature, to reduce porosity and enhance material consistency. Future work should focus on developing more precise models that incorporate the effects of porosity, enabling better predictions of material properties like Young's modulus and density for FG beams produced via powder metallurgy.

The promising potential applications of FGMs, owing to their exceptional properties that traditional manufacturing methods struggle to replicate, are expanding rapidly. While significant advancements have been made in the past decade, challenges remain, particularly in scaling laboratory-grade fabrication techniques to industrial production levels. Overcoming these challenges is crucial for the broader implementation of FGMs in engineering applications.

Additional Information

Author Contributions

All authors have reviewed the final version to be published and agreed to be accountable for all aspects of the work.

Concept and design: Pravin Malik, Ravikiran Kadoli, Sharnappa Joladarashi, Permi Jagadish

Acquisition, analysis, or interpretation of data: Pravin Malik, Permi Jagadish

Drafting of the manuscript: Pravin Malik, Permi Jagadish

Critical review of the manuscript for important intellectual content: Pravin Malik, Ravikiran Kadoli, Sharnappa Joladarashi

Supervision: Ravikiran Kadoli, Sharnappa Joladarashi

Disclosures

Human subjects: All authors have confirmed that this study did not involve human participants or tissue. **Animal subjects:** All authors have confirmed that this study did not involve animal subjects or tissue. **Conflicts of interest:** In compliance with the ICMJE uniform disclosure form, all authors declare the following: **Payment/services info:** All authors have declared that no financial support was received from any organization for the submitted work. **Financial relationships:** All authors have declared that they have no financial relationships at present or within the previous three years with any organizations that might have an interest in the submitted work. **Other relationships:** All authors have declared that there are no other relationships or activities that could appear to have influenced the submitted work.

References

1. Gupta A, Talha M: Recent development in modeling and analysis of functionally graded materials and structures. Progress in Aerospace Sciences. 2015, 79:1-14. 10.1016/j.paerosci.2015.07.001
2. Kieback B, Neubrand A, Riedel H: Processing techniques for functionally graded materials. Materials Science and Engineering A. 2003, 362:81-106. 10.1016/s0921-5093(03)00578-1
3. Sobczak JJ, Drenchev L: Metallic functionally graded materials: a specific class of advanced composites. Journal of Material Science and Technology. 2013, 29:297-316. 10.1016/j.jmst.2013.02.006
4. Naebe M, Shirvanimoghaddam K: Functionally graded materials: a review of fabrication and properties. Applied Materials Today. 2016, 5:223-45. 10.1016/j.apmt.2016.10.001
5. Lambros J, Narayanaswamy A, Santare M, Anlas G: Manufacture and testing of a functionally graded material. Journal of Engineering Materials and Technology. 1999, 121:488-93. 10.1115/1.2812406
6. Saleh B, Jiang J, Fathi R, et al.: 30 Years of functionally graded materials: an overview of manufacturing methods, applications and future challenges. Composites Part B Engineering. 2020, 201:108376. 10.1016/j.compositesb.2020.108376
7. Boggarapu V, Sreekanth PSR, Peddakondigalla VB: Microstructure, mechanical and tribological properties of Al/Cu functionally graded material fabricated through powder metallurgy. Journal of Engineering Research. 2024, 12:502-10. 10.1016/j.jer.2023.100119

8. Gupta P, Kumar D, Parkash OM, Jha AK: Structural and mechanical behaviour of 5% Al2O3-reinforced Fe metal matrix composites (MMCs) produced by powder metallurgy (P/M) route. Bulletin of Materials Science. 2013, 36:859-68. 10.1007/s12034-013-0545-1
9. Bhattacharyya M, Kumar AN, Kapuria S: Synthesis and characterization of Al/SiC and Ni/Al2O3 functionally graded materials. Materials Science and Engineering A. 2008, 487:524-35. 10.1016/j.msea.2007.10.040
10. Matuła I, Dercz G, Barylski A, Kubisztal J: Porous functionally graded material based on a new Ti-25Nb-5Zr-(2Sn) alloy produced using the powder metallurgy technique. Journal of Alloys and Compounds. 2024, 982:173779. 10.1016/j.jallcom.2024.173779
11. Phani KK, Niyogi SK: Young's modulus of porous brittle solids. Journal of Materials Science. 1987, 22:257-63. 10.1007/bf01160581
12. Asmani M, Kermel C, Leriche A, Ourak M: Influence of porosity on Young's modulus and Poisson's ratio in alumina ceramics. Journal of the European Ceramic Society. 2001, 21:1081-86. 10.1016/s0955-2219(00)00314-9
13. Kováčik J: Correlation between Young's modulus and porosity in porous materials. Journal of Materials Science Letters. 1999, 18:1007-10. 10.1023/a:1006669914946
14. Chawla N, Deng X: Microstructure and mechanical behavior of porous sintered steels. Materials Science and Engineering A. 2005, 390:98-112. 10.1016/j.msea.2004.08.046
15. Savchenko N, Sevostyanova I, Sablina T, Gömze L, Kulkov S: The influence of porosity on the elasticity and strength of alumina and zirconia ceramics. AIP Conference Proceedings. 2014, 1623:547-550. 10.1063/1.4899003
16. Wattanasakulpong N, Ungbhakorn V: Linear and nonlinear vibration analysis of elastically restrained ends FGM beams with porosities. Aerospace Science and Technology. 2014, 32:111-20. 10.1016/j.ast.2013.12.002
17. Kapuria S, Bhattacharyya M, Kumar AN: Bending and free vibration response of layered functionally graded beams: a theoretical model and its experimental validation. Composite Structures. 2008, 82:390-402. 10.1016/j.compstruct.2007.01.019
18. Wattanasakulpong N, Prusty BG, Kelly DW, Hoffman M: Free vibration analysis of layered functionally graded beams with experimental validation. Materials & Design (1980-2015). 2012, 36:182-90. 10.1016/j.matdes.2011.10.049
19. Malik P, Kadoli R: Nonlinear bending and free vibration response of SUS316-Al2O3 functionally graded plasma sprayed beams: theoretical and experimental study. Journal of Vibration and Control. 2016, 24:1171-84. 10.1177/1077546316659422
20. Demir C, Oz FE: Free vibration analysis of a functionally graded viscoelastic supported beam. Journal of Vibration and Control. 2014, 20:2464-86. 10.1177/1077546313479634
21. Liu J: Processes for sintering aluminium and aluminium alloy components. Google Patents, 2009.
22. Pieczonka T, Kazior J: Sintering atmosphere effects on the densification of Al-SiC compacts. International Journal of Materials and Metallurgical Engineering. 2014, 8:252-55.
23. Phani KK, Niyogi SK: Porosity dependence of ultrasonic velocity and elastic modulus in sintered uranium dioxide — a discussion. Journal of Materials Science Letters. 1986, 5:427-30. 10.1007/bf01672350